A three-dimensional simulation and process analysis of tropospheric Ozone Depletion Events (ODEs) during the springtime of Arctic using CMAQ

Simeng Li[1], Le Cao[1], Yicheng Gu[1], and Yuhan Luo[2]

[1]Key Laboratory for Aerosol-Cloud-Precipitation of China Meteorological Administration, Nanjing University of Information Science and Technology, Nanjing, 210044, China
[2]Key Laboratory of Environmental Optics and Technology, Anhui Institute of Optics and Fine Mechanics, Chinese Academy of Sciences, Hefei, 230031, China

Correspondence: Le Cao (le.cao@nuist.edu.cn)

Abstract. The tropospheric Ozone Depletion Event (ODE), first observed at Barrow (now known as Utqiagvik), Alaska, is a phenomenon that frequently occurs during the springtime of Arctic. In the present study, we performed a three-dimensional model study on ODEs occurring at Barrow and its surrounding areas between March 28th and April 6th, 2019, using a 3-D multi-scale air quality model, CMAQ. Several ODEs observed at Barrow were successfully captured and two of them were

5   analyzed thoroughly using process analysis. We found that the ODE occurring between March 30th and 31st, 2019 (referred to as ODE1) was caused mainly by a horizontal transport of an ozone-lacking air from the Beaufort sea to Barrow. This ozone-lacking air was formed due to a release of sea-salt aerosols from the Bering Strait under a strong wind condition, resulting from a cyclone generated at the Chukotka Peninsula. It was also found that over the Beaufort sea, the surface ozone drops to a level lower than 5 ppb, and the local chemistry contributed as large as 10 ppb to the ozone loss. Moreover, BrO over the sea

10   was found to attain a maximum of approximately 100 ppt. This ozone-lacking air over the sea was horizontally transported to Barrow, leading to the occurrence of ODE1. Regarding another ODE on April 2nd (ODE2), we found its occurrence also dominated by the horizontal advection from the sea, but under the control of an anti-cyclone. The termination of this ODE was attributed to the replenish of ozone-rich air from the free troposphere by a strong vertical transport.

1 Introduction

15   Ozone, one of the most important atmospheric constituent in the atmosphere of Arctic, has historically attracted much attention from the scientific community. In the Arctic, due to the lack of human activities, the tropospheric ozone remains at background level, 40-60 ppbv (Seinfeld and Pandis, 2016). However, Oltmans (1981) observed an abnormal decrease of surface ozone at Barrow (now known as Utqiagvik, 71.3230° N, 156.6114° W), Alaska in the springtime. The surface ozone was found to drop from the background level to a few ppbv, within a couple of days or even hours, which is called ozone depletion event (ODE).

20   After that, Barrie et al. (1988) found that the tropospheric ODE is formed due to the occurrence of an auto-catalytic reaction cycle involving bromine chemistry, of which the major reactions are shown below (Barrie et al., 1988; Platt and Hönninger,

2003; von Glasow and Crutzen, 2014):

$$Br + O_3 \rightarrow BrO$$

$$BrO + BrO \rightarrow \begin{cases} 2Br + O_2 \\ Br_2 + O_2 \end{cases} \tag{I}$$

25 $Br_2 + h\nu \rightarrow 2Br.$

$$Net : 2O_3 \rightarrow 3O_2.$$
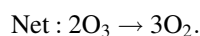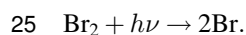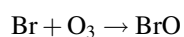
In this reaction cycle, the total amount of Br and BrO keeps constant, which means that these bromine species play as catalysts. Aside from reaction cycle (I), Br and BrO can also react with HO_2 radicals, forming HBr and HOBr, respectively. HBr and

30 HOBr are relatively inert, so that the formation of these two species tends to terminate the reaction cycle. HBr can also be generated from reactions between Br atoms and olefins or aldehydes (Platt and Hönninger, 2003), then leaves the atmosphere due to its tendency to dissolve (Platt and Hönninger, 2003) .

However, heterogeneous reactions taking place at the surface of substrates (such as frost flowers or sea-salt aerosols) lead to the liberation of the inert bromine (McConnell et al., 1992; Fan and Jacob, 1992), which is essential for the re-emissions

35 of bromine, the so-called "bromine explosion" mechanism (Platt and Lehrer, 1997; Wennberg, 1999). The main reaction is as follows:

$$HOBr(g) + Br^-(l) + H^+(l) \rightarrow Br_2(g) + H_2O(l). \tag{R1}$$

Reaction (R1) represents one of these heterogeneous reactions, which forms active Br_2 from bromine ions (Br^-). Also, a similar heterogeneous reaction involving Cl^- also occurs:

40 $$HOBr(g) + Cl^-(l) + H^+(l) \rightarrow BrCl(g) + H_2O(l), \tag{R2}$$

to form another active bromine species, BrCl. Therefore, additional bromine can be rapidly released into the atmosphere, causing a fast ozone depletion in the boundary layer. Under this condition, the major oxidant in the atmosphere shifts from ozone to bromine species. Because the bromine species are capable of accelerating the deposition of mercury from the air, more mercury can enter into the ocean, and then influence the biosphere through marine wildlife (Simpson et al., 2007; Steffen

45 et al., 2008).

Many researchers have contributed to the study of ODEs. Observations and experiments were made to establish the internal relationship between the ozone depletion and the bromine explosion (Oltmans, 1981; Barrie et al., 1988; Bottenheim et al., 1990; McConnell et al., 1992; Fan and Jacob, 1992; Hausmann and Platt, 1994; Boylan et al., 2014). Moreover, scientists also tried to reproduce ODEs using parameterizations or model simulations. To name a few, Lehrer et al. (2004) used an one-

50 dimensional model to identify weather conditions and underlying surface properties necessary for the occurrence of ODEs. They concluded that the sunlight, bromine-containing surface, strong conversion on the top of boundary layer are essential

conditions for the occurrence of ODEs. Only in spring can these conditions be satisfied, which is the reason that ODEs were mostly observed in the springtime. Thomas et al. (2011, 2012) studied the chemistry on the snow at Summit, Greenland using a one-dimensional atmospheric boundary layer model named MISTRA-SNOW. They concluded that the bromine- and nitrate-

55 containing surfaces help to maintain the concentrations of NO and BrO during the study time.

The first three-dimensional simulation of ODEs was implemented by Zeng et al. (2003, 2006), who found approximately 60% of the northern high altitudes covered by a low surface ozone (<20 ppbv) and a high BrO. Zeng et al. also concluded that there exists a strong anti-correlationship between the tropospheric BrO and the surface temperature. Besides, they found that the concentration of BrO is relevant to movements of air masses and the variation of the temperature rather than the absolute

60 value of the temperature. Later, by using a global chemistry transport model, p-TOMCAT, Yang et al. (2008, 2010, 2019) proposed that the bromine in polar area mostly comes from sea-salt aerosols. A release of active bromine into the atmosphere then results in an average of 8% of the tropospheric ozone loss.

Recently, Herrmann et al. (2021, 2022) and Marelle et al. (2021) tried to reproduce ODEs using a mesoscale forecasting model WRF-Chem. These studies are a major advance in 3-D simulations of ODEs. In the study of Herrmann et al., they

65 concluded that the bromine explosion mechanism alone is unable to maintain enough BrO. Instead, a heterogeneous reaction involving ozone and bromine ions makes the bromine explosion possible. Moreover, Marelle et al. found that the surface snow and blowing snow are both able to initialize the ODEs. It was suggested by Marelle et al. that, although blowing snow is the major source of sea-salt aerosols, it exerts a weak impact on ODEs. Both of these two studies contribute largely to the 3-D simulations of ODEs.

70 However, in previous simulations of ODEs, due to the use of self-constructed chemical mechanisms without validations, uncertainties may be induced into chemical simulations. Moreover, contributions of physical and chemical processes to the occurrence of ODEs need to be studied more thoroughly. Therefore, in this study, we conducted simulations of ODEs using a 3-D multi-scale air quality model, CMAQ (Community Multiscale Air Quality Modeling System), focusing on Barrow and surrounding areas (see Fig. 1a). We also used a validated chemical mechanism originally instrumented in CMAQ,

75 CB05eh51_ae6_aq, which considers the halogen chemistry (Sarwar et al., 2015; Sherwen et al., 2016; Yarwood et al., 2012). In addition, we performed a process analysis (Gipson, 1999) to estimate the contribution from each physical or chemical process to the variations of ozone and bromine species during ODEs. By doing that, we were able to quantitatively analyze the variations of the selected species and the importance of influencing factors for ODEs.

In the following sections, we will introduce the configurations of our simulations in Sect. 2, and then present the validations

80 and quantitative analysis of two ODEs in Sect. 3. At last, conclusions and future work are given in Sect. 4.

2 Observational Data and Model Settings

In this study, the CMAQ model (US EPA Office of Research and Development, 2018) was used to reproduce the ODEs. The WRF model (Weather Research and Forecasting, Skamarock et al., 2008) was used to capture the meteorological parameters

| (a) The geographical map | (b) The computational domain |
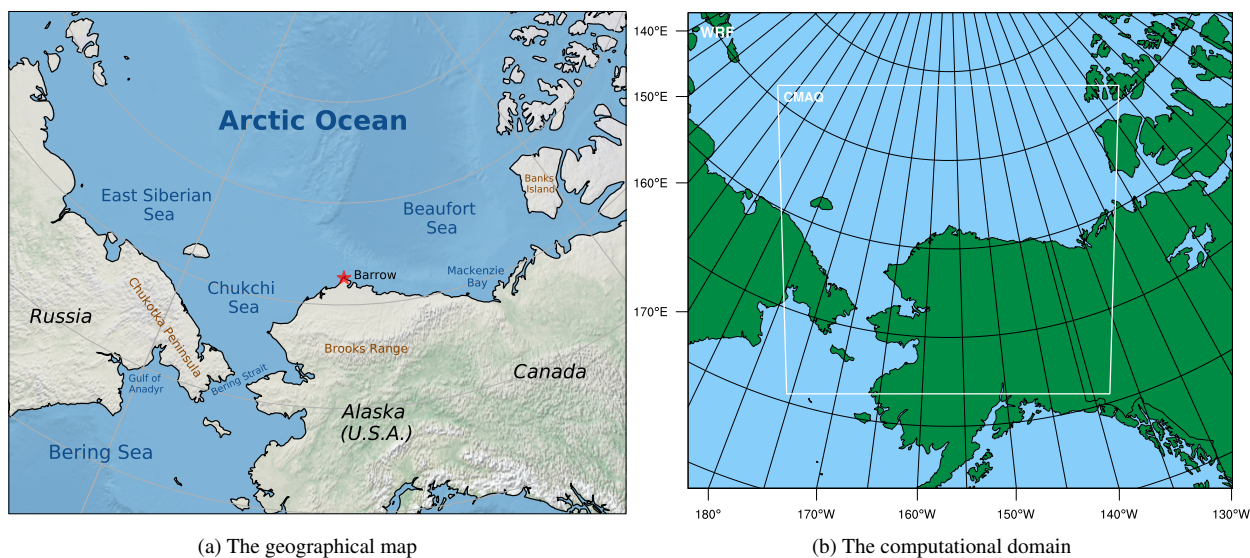
Figure 1. The geographical map of the research area and the computational domain used in WRF and CMAQ .

and drive the CMAQ model. Hourly observational data of in-situ meteorological parameters and ozone were also used to

85 validate the simulations.

2.1 Model Settings

CMAQ requires the input of meteorological fields including temperature, wind and pressure to drive the chemical simulations. In this study, outputs of WRF model were used to drive the CMAQ model.

2.1.1 WRF

90 The WRF model version 3.9.1, developed by National Center for Atmospheric Research (NCAR) and National Oceanic and Atmospheric Administration (NOAA), was used to capture the meteorological fields (Skamarock et al., 2008). The initial conditions and boundary conditions of WRF were given by GDAS/FNL (the Global Data Administration System / Final) re-analysis dataset (National Centers for Environmental Prediction et al., 2015), with a spatial resolution of $0.25° \times 0.25°$ and a temporal resolution of 6 h. The computational domain used in WRF and CMAQ is shown in Fig. 1(b), of which the center

95 is $70.0°$ N, $156.8°$ W. The spatial resolution was set to 9km. Along the vertical direction, 35 layers were distributed. The time period of the WRF simulation ranges from March 25th to April 10th, 2019. The detailed settings of the WRF model are given in Table 1.

Table 1. Configurations of WRF and CMAQ in the present study.

Options	Settings	References
	WRF	
Microphysics	Thompson scheme	Thompson et al. (2008)
Boundary-layer model	Mellor-Yamada-Janjic scheme	Janjić (1994)
Land surface model	Noah land-surface model	Chen et al. (1997)
Surface-layer model	Monin-Obukhov (Janjic Eta) similarity scheme	Janjić (1994)
Cumulus parametrization	Modifed Tiedtke scheme	Tiedtke (1989)
Longwave radiation	LW RRTMG scheme	Iacono et al. (2008)
Shortwave radiation	SW RRTMG scheme	Iacono et al. (2008)
Time period	March 25th - April 10th, 2019	
Spatial resolution	9×9 km	
Vertical layers	35 levels	
	CMAQ	
Chemical mechanism	CB05eh51_ae6_aq	Sarwar et al. (2015)
Emissions	EDGAR version 5.0	Crippa et al. (2020)
Boundary conditions	CAM-Chem (adjusted)	Buchholz et al. (2019)
Heterogeneous reactions	HOBr + ASEACAT = Br_2 +H_2O + ASEACAT	Based on Mellberg (2014)
Initial conditions	Profile (build-in)	
Time period	March 28th - April 6th, 2019	

2.1.2 CMAQ

In this study, a 3-D regional air quality model, CMAQ, developed by the United States Environmental Protection Agency
100   (EPA), was used to capture the ODEs. CMAQ combines atmospheric science and air quality models together and uses multi-processor technology for three-dimensional simulations of ozone, particulate matters and acid deposition (US EPA Office of Research and Development, 2020). In the present study, CMAQ versions 5.2.1 (US EPA Office of Research and Development, 2018) was used to capture the variation of ozone and other atmospheric constituents during ODEs. The equation denoting the change of each chemical species in CMAQ is shown below:

105    $$\frac{\partial c}{\partial t} = \text{Adv} + \text{Diff} + R_c + E_c + S_c \qquad (1)$$

In Eqn. (1), $\frac{\partial c}{\partial t}$ denotes the temporal change of the chemical species. The terms on the right hand side of Eqn. (1) represent advection, diffusion, chemical conversion of species c, emissions of species c, and loss of species c, respectively (US EPA Office of Research and Development, 2018). The time period simulated in CMAQ ranges from March 28th to April 6th, 2019. More details of the CMAQ configuration can be found in Table 1.

110   The chemical mechanism originally instrumented in CMAQ, CB05eh51_ae6_aq, was used in this study, which considers
the halogen chemistry (Sarwar et al., 2015; Sherwen et al., 2016; Yarwood et al., 2012). A complete listing of reactions in
this mechanism can be found in https://github.com/USEPA/CMAQ/blob/5.2.1/CCTM/src/MECHS/cb05eh51_ae6_aq/mech_
cb05eh51_ae6_aq.def. However, the important heterogeneous reaction that determines the bromine explosion mentioned above
is still lacking in this mechanism. Thus, we added one reaction into this mechanism:

115     $HOBr + ASEACAT \rightarrow Br_2 + H_2O + ASEACAT$ (R3)

In Reaction (R3), ASEACAT represents the number concentration of sea-salt aerosols in the model. Based on the study of
Mellberg (2014), a reaction coefficient $k = 2.5 \times 10^{-14}$ molecules$^{-1} \cdot$ cm$^3 \cdot$ s^{-1} was given to Reaction (R3) in the mechanism.
This reaction coefficient used in the present study is one order larger than that proposed by Mellberg (2014). It is because that
in the study of Mellberg, bromine concentrations were underestimated by 5 to 10 times. Furthermore, only using this reaction
120   coefficient can result in a reasonable simulation of ODEs in the present study.

        In addition, we found that in simulations, ozone and other species in the computational domain can be greatly affected
by the implemented boundary conditions. Thus, we used a time-dependent boundary condition adapted from outputs of an
earth system model, the Community Atmosphere Model with Chemistry (CAM-Chem) (Buchholz et al., 2019). However, the
chemical mechanism used in CAM-Chem does not consider the influence of the bromine explosion mechanism (Emmons et al.,
125   2020). Therefore, we modified the boundary conditions of ozone according to observations. For the ozone in the boundary layer,
if it is on the surface of sea ice, ozone was set to 3 ppbv; if it is over the sea, ozone was set to 10 ppbv; if it is at a coastal area,
ozone was set to 15 ppbv. Furthermore, because the free atmospheric ozone can also be remarkably affected by the bromine
explosion and the ODEs, ozone in the free troposphere in the implemented boundary condition was also reduced to half of
the original value to consider the influence of the bromine explosion. The detailed settings of the boundary conditions can be
130   found in Section *Code and data availability*.

        The emissions used in CMAQ were generated by Sparse Matrix Operator Kernel Emissions (SMOKE) developed by EPA
(Baek and Seppanen, 2019). EDGAR (Emissions Database for Global Atmospheric Research) version 5.0 was implemented
in SMOKE as the emission inventory (Crippa et al., 2018, 2020; Pesaresi et al., 2019; Monforti-Ferrario et al., 2019). A surf
zone of 50 m was also set up in the present model, due to the existence of ocean in our computational domain. By doing that,
135   more sea spray can be released from the surf zone.

        Aside from studying the temporal variation of chemical species, we also used PA, i.e., process analysis (Gipson, 1999), to
estimate the contribution from each physical or chemical process to the variation of a selected air constituent. PA is a module
originally included in CMAQ. By performing PA, we were able to analyze the changes of the selected species and quantitatively
assess the importance of influencing factors. Integrated Process Rate (IPR) and Integrated Reaction Rate (IRR) were calculated
140   in the PA module. The former includes the net change of species through advection, diffusion, emissions, deposition, and
the overall effect of chemical process. The latter calculates the variation caused by each chemical reaction in the mechanism
(Gipson, 1999).
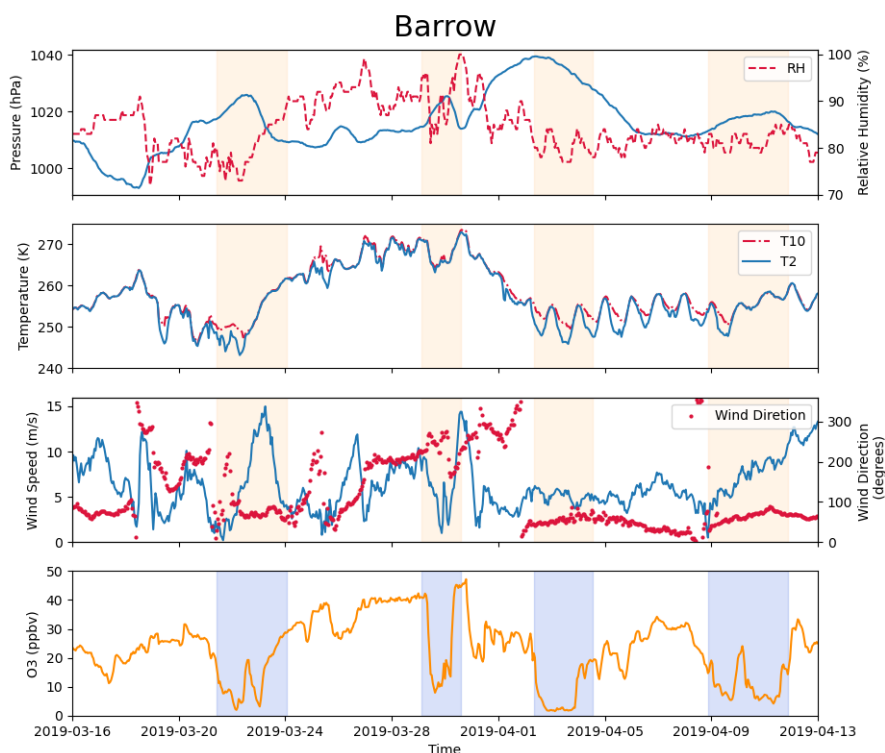
Figure 2. The observational data of pressure, relative humidity, temperature at 2 m and 10 m, wind direction, wind speed at 10 m and surface ozone at Barrow (now known as Utqiagvik) from March 16th to April 13th, 2019. The shaded areas denote the occurrence of complete ODEs, of which the minimal ozone is less than 10 ppb.

2.2 Observational Data

The observational data were obtained from the Global Monitoring Laboratory (GML, https://gml.noaa.gov/aftp/data/barrow/),

145 which belongs to National Oceanic and Atmospheric Administration (NOAA). The observational data included surface ozone (McClure-Begley et al., 2014) and meteorological parameters such as wind direction, wind speed at 10 m, pressure, temperature at 2 m and 10 m, and relative humidity (Mefford et al., 1996; Herbert et al., 1986a, b, 1990, 1994). In this study, we focused on the spring of 2019, of which the observational data are shown in Fig. 2. We chose March 25th to April 10th, 2019 for simulation. In this time period, several complete ODEs, of which the minimal ozone is less than 10 ppb, are included (see

150 the shaded areas in Fig. 2). Synoptic charts during this period with the surface analysis were also obtained from the Weather Prediction Center, shown in the supplements.

To validate the simulations, we used the Pearson correlation coefficient (R) and the root-mean-square error (RMSE) calculated as follows:

$$R = \frac{\sum_{i=1}^{N}\left(S_i - \overline{S}\right)\left(O_i - \overline{O}\right)}{\sqrt{\sum_{i=1}^{N}\left(S_i - \overline{S}\right)^2 \sum_{i=1}^{N}\left(O_i - \overline{O}\right)^2}}, \tag{2}$$

155

$$RMSE = \sqrt{\frac{\sum_{i=1}^{N}\left(S_i - O_i\right)^2}{N}}. \tag{3}$$

In Eqns. (2) and (3), S_i and O_i represent the simulated value and the observed value at the ith time points, respectively. N represents the total number of time points. $\overline{S}$ and $\overline{O}$ stand for the time-averaged values during this time period, correspondingly. R ranges from -1 to 1. The closer the absolute value of R is to 1, the better simulations match the observational data. For RMSE, a smaller RMSE represents a less deviation between simulations and observations.

160 The detailed simulation results are shown in the following section.

3 Results and Discussions

In this section, we will demonstrate the reliability of the simulations first, and then discuss the simulated ODEs in detail. At last, a comprehensive process analysis of each ODE was conducted. All geographic names mentioned in the following content can be found in Fig. 1(a).

165 ### 3.1 Validation of the simulations

The temporal variation of the meteorological field (including temperature, horizontal components of the wind speed, and pressure) in Barrow simulated by WRF was compared with the observational data, shown in Fig. 3. It can be seen that during this period, the pressure of Barrow (71.3230° N, 156.6114° W) is generally in a trend of first increasing and then decreasing, with an obvious abrupt decrease from March 30th to 31st (Fig. 3a). This significant decline of the pressure corresponds to a

170 remarkable drop in temperature and a rapid change in the horizontal components of wind speed, U and V (see Fig. 3c and d). All the statistical parameters can be found in Table S1 of the supplementary material. The coefficients (R) of pressure, temperature, U and V between simulations and observations are 0.991, 0.92, 0.881 and 0.897, respectively. The RMSEs of pressure, temperature, U and V are 3.081 hPa, 3.784 K, 2.153 m/s and 2.282 m/s, respectively. Thus, we can conclude that the simulated meteorological field is accurate, so that it can be used to drive the chemical simulations of CMAQ during this time.

175 The temporal variation of the surface ozone in Barrow simulated by CMAQ was then compared with the observational data, shown in Fig. 4. During this period, the surface ozone changed dramatically, and three ODEs were observed.

1. On March 29th, from 07 to 16 UTC, ozone declined from 41.6 ppb to 9.0 ppb, then on March 30th from 05 to 10 UTC, ozone recovered from 13.6 ppb to 45.2 ppb.
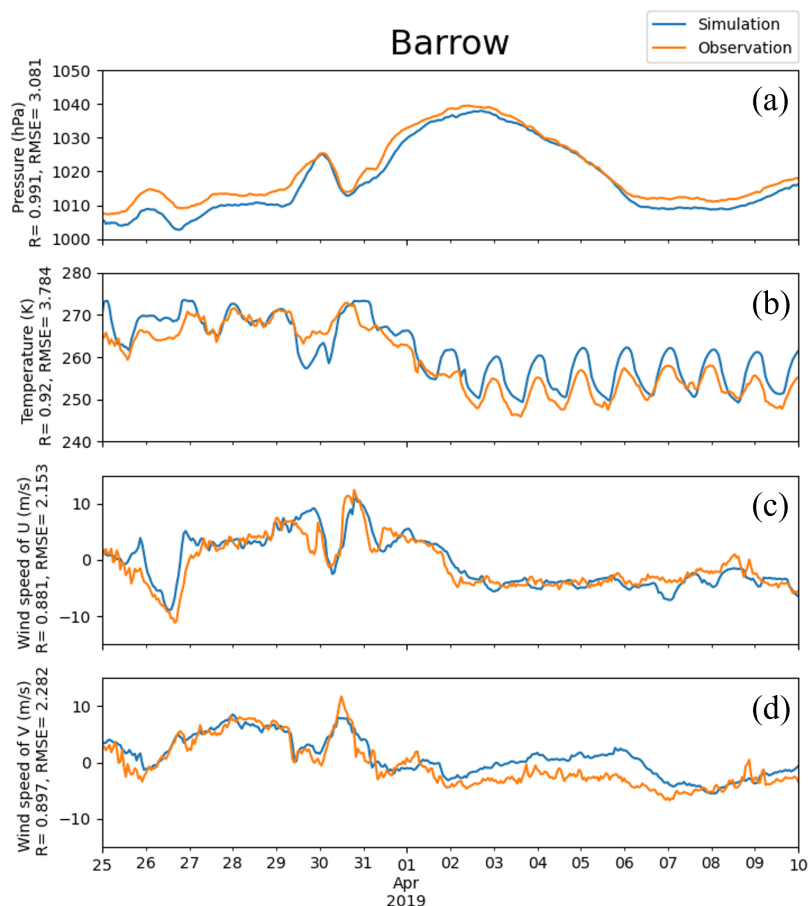
Figure 3. Meteorological fields obtained from simulations and observations in Barrow from March 25th to April 10th, 2019. The correlation coefficient R and the root-mean-square error RMSE were also presented in the vertical axis.

2. Later, from 19 UTC on March 30th to 04 UTC on March 31st, a partial ODE occurred. The surface ozone declined from 47.2 ppb to 19.9 ppb. Then at 10 UTC on March 31st, ozone recovered from 18.7 ppb to 32.6 ppb within three hours.

3. A complete ODE occurred on April 2nd. From 05 UTC to 22 UTC, ozone decreased from 28.4 ppb to 1.8 ppb. After a whole day of low values, ozone resumed from 2.8 ppb to 17.9 ppb.

The correlation coefficient and the root-mean-square RMSE of the surface ozone between the simulations and the observations are 0.793 and 8.407 ppb, respectively. The trend of the surface ozone was also well reproduced (see Fig. 4), including those dramatic changes discussed above. In particular, ODEs on March 29th, March 31st, and April 2nd were captured, not only the start of the ODEs, but also the recovery of them. It enables us for the subsequent analysis. It should be noted that although our simulations fit the observations well, there still exist a fraction of mismatches, possibly due to the uncertainty in boundary conditions. For example, due to the particularity of the ODE on March 29th, ozone over the Chukotka Peninsula
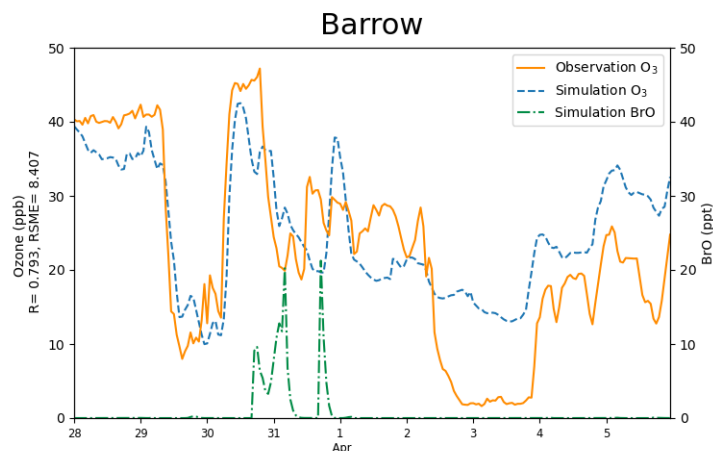
Figure 4. The surface ozone (ppb) obtained from simulations and observations together with the simulated BrO in Barrow from March 28th to April 5th, 2019. The correlation coefficient R and the root-mean-square error RMSE were also presented in the vertical axis.

(66.8° N, 176.6° W) in the implemented boundary conditions was adjusted to 40 % of its original value. Simulation results without this adjustment are shown in Fig. S1 in the supplement. It can be seen that without this adjustment, the simulated ozone on March 29th would be largely different from the observations.

3.2 Comprehensive analysis of each ODE

In the previous section, we mentioned that during this period, the pressure of Barrow is generally in a trend of first increasing and then decreasing, with an obvious abrupt decrease from March 30th to 31st (Fig. 3a). These meteorological changes at Barrow mainly resulted from two weather conditions, a cyclone and an anti-cyclone, respectively. Under these circumstances, three ODEs occurred. From our simulations, we found that the ODE occurring on March 29th in Barrow mainly formed by a transport of low-ozone air masses to the west of the Chukchi Sea (71.7° N, 169.9° W), so that the simulation of this ODE is heavily determined by the applied boundary conditions of the model. Thus, we will not investigate it deeper in this study. The following two ODEs, occurring on March 31st (named as ODE1) and April 2nd (named as ODE2), will be analyzed in detail below.

3.2.1 ODE1 (on March 31st)

The spatial distribution of the surface temperature and the pressure from March 30th to March 31st was shown in Fig. 5. Globally, during this period, the Arctic Ocean (79.0° N, 156.9° W) was dominated by the Arctic vortex, of which the center pressure was low (1002 hPa) and the center temperature was less than -24°C. In contrast, the mainland of Alaska was covered by a uniform pressure field. Figure 5(a) shows that at UTC 00 on March 30th, the gradient of the air temperature on the Beaufort Sea (73.7° N, 146.6° W) was very large. This large temperature gradient was formed due to the passing by of a
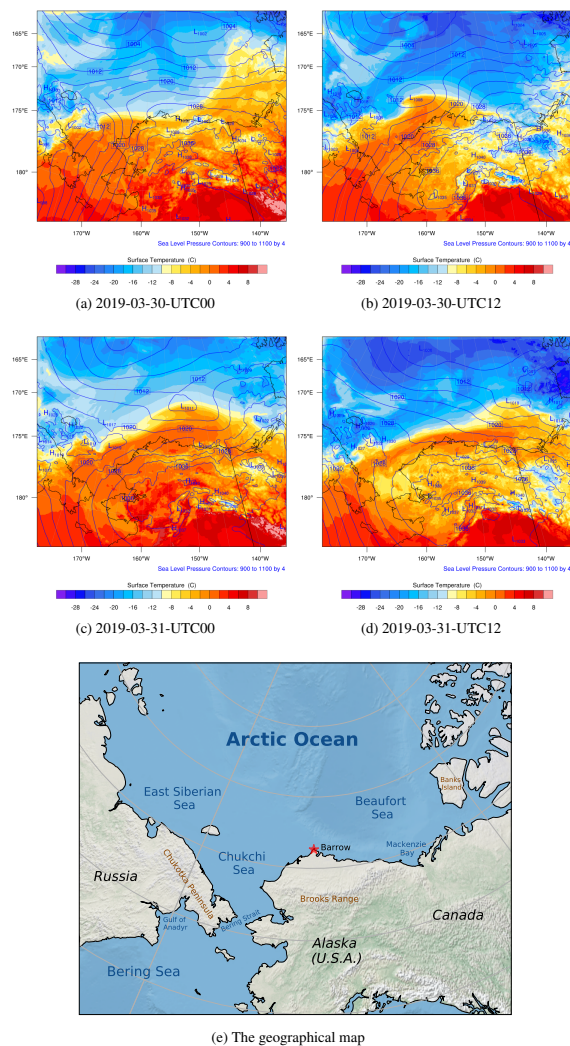
Figure 5. The spatial distribution of the sea level pressure (hPa, contour lines) and surface temperature (°C, contour fills) simulated by WRF from March 30th to March 31st, 2019.

cold front in this area (see Fig. S2b in the supplements denoting the weather patterns). At the same time, the temperature field around the Chukotka Peninsula became twisted (see also Fig. 5a). A low-pressure system (i.e., a cyclone) was also formed over the Chukchi Sea. Then, the low-pressure system developed rapidly and moved northeastward. Meanwhile, the meteorological field around the cyclone was distorted accordingly, especially the temperature. At 12 UTC on March 30th shown in Fig. 5(b), the center of the low-pressure system reached 1008 hPa. This low pressure system also generated a cold font on the left and a stationary front on the right (see Fig. S2d in the supplements), leading to a strong temperature gradient around this low pressure. Then, at 00 UTC on March 31st (Fig. 5c), the low-pressure system moved to the north of Barrow, and its center pressure
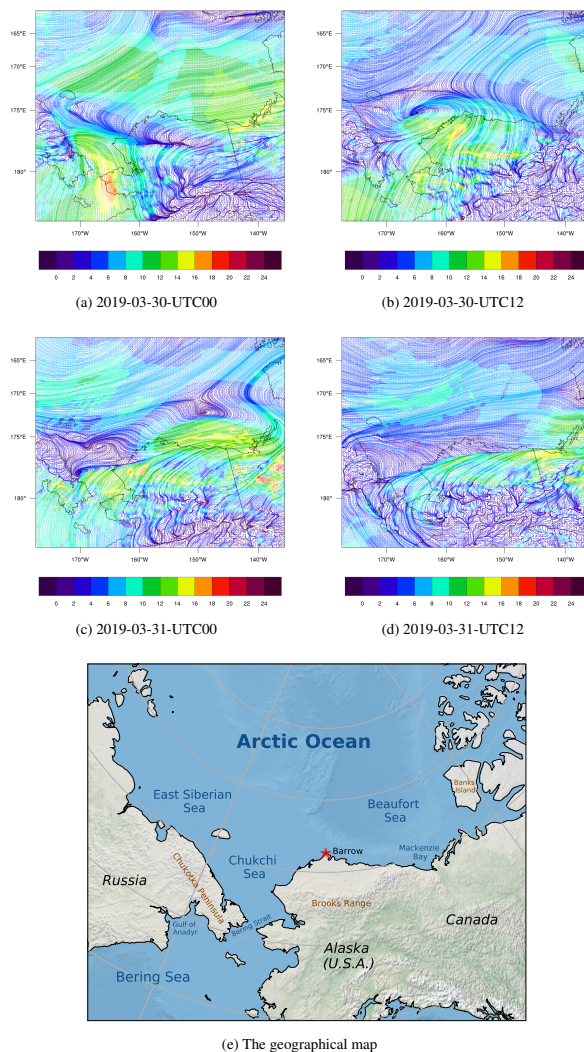
Figure 6. The spatial distribution of surface wind (m/s) and the streamline simulated by WRF from March 30th to March 31st, 2019.

increased to 1011 hPa, which means the weakening of the low-pressure system. Within a couple of hours (see Fig. 5d), the
215 cyclone continued moving eastward, but a front remained over the sea. For the meteorological field with a finer time interval, please refer to Fig. S3 in the supplements.

The spatial distribution of the surface wind from March 30th to March 31st is shown in Fig. 6. Figure 6(a) shows that at 00 UTC on March 30th, the wind speed over the Bering Strait (66.0° N, 168.9° W) was very large, of which the maximum reached 18 m/s. With such a high wind speed, sea-salt aerosols can be rapidly released into the atmosphere (see Fig. S4b in
220 the supplements). The liberation of sea-salt aerosols causes a release of the reactive bromine into the atmosphere, which can deplete the surface ozone. At UTC12 on March 30th shown in Fig. 6(b), the wind was cyclonic over the Chukchi Sea and the

wind speed was quite large between the two fronts mentioned above. Then, in Fig. 6(c), at UTC 00 on March 31st the cyclone moved eastward and the wind speed decreased. After 12 hours (see Fig. 6d), the wind speed in this area was low. The cyclone moved to the south of the Banks Island (73.48° N, 121.8° W), which indicates the end of this process. For the surface wind
225 with a finer time interval, please refer to Fig. S5 in the supplements. This process is similar to the "bromine cyclone transport event" described by Blechschmidt et al. (2016), but the scale of the process discussed in this study is smaller than that of Blechschmidt et al. (2016).

The spatiotemporal distribution of the simulated ozone and BrO on March 30th is shown in Fig. 7. We mentioned above that under the high-wind-speed conditions, a large amount of sea-salt aerosols can be carried into the atmosphere, as early
230 as March 29th (see Fig. S4a in the supplements). However, changes in ozone and BrO were not revealed until 00 UTC on March 30th, which means that the response of the chemical field to the change in meteorology is retarded. Figure 7(a) shows that, over the Arctic Ocean, the surface ozone was at a low level at UTC 00 on March 30th. In contrast, over the mainland of Alaska, the surface ozone remained at a background level. BrO is an indicator of ODEs because it increases rapidly during the depletion of ozone. Thus, when ozone at the Gulf of Anadyr (64.4° N, 178.2° W) and the north of Banks Island began
235 to decrease (Fig. 7a and b), the surface BrO started to generate, shown in Fig. 7(e). In the next 4 hours, the surface ozone at the Bering Strait continued its depletion shown in Fig. 7(c). Meanwhile, BrO at this place is explosively generated, shown in Fig. 7(f) and (g). The maximum of BrO over the Bering Strait was larger than 100 ppt, of which the high value areas were consistent with the region abundant in sea-salt aerosols (Fig. S4 in the supplements). Then, under the control of the strong wind, the air mass with depleted ozone and abundant bromine moved northeastward. Moreover, because of the cyclonic wind
240 discussed above, the air mass containing the depleted ozone and abundant bromine was twisted (see Fig. 7c and g). At UTC 06 on March 30th, the sunset occurred. The low-ozone area stopped expanding. The high-BrO area also disappeared due to the absent of the photolysis of Br$_2$.

The spatiotemporal distribution of the surface ozone and BrO from March 30th to 31st was also shown in Fig. 8. At UTC22 on March 30th shown in Fig. 8(a), the sun rose again and the photochemistry started. It can be seen in Fig. 8(a) and (b) that the
245 chemical field of ozone was twisted strongly, under the cyclonic wind on the north of Barrow. Meanwhile, the reactive bromine returned to the atmosphere by the bromine explosion mechanism, shown in Fig. 8(e). Then at 00 and 02 UTC on March 31st (see Fig. 8f and g), BrO increased explosively over time. Within 4 hours, the mixing ratio of BrO reached a maximum larger than 100 ppt over the Beaufort Sea, which is consistent with the spatial distribution of sea-salt aerosols (see Fig. S4f and g in the supplements). Correspondingly, the surface ozone decreased continuously (see Fig. 8c), but the decrease was slightly
250 behind the increase of BrO. The mixing ratio of the surface ozone had been as low as 10 ppb over the north of the Mackenzie Bay (69.7° N, 137.1° W). At 04 UTC on March 31st (see Fig. 8h), the source of BrO was again cut off due to the sunset. The amount of BrO in areas where the sunset occurred was much lower than that in which the sunset did not occur. In contrast, the change in the surface ozone is a little bit retarded. The minimum of the surface ozone at UTC02 on March 31st (∼5 ppb over the north Mackenzie Bay, see Fig. 8d) was even lower than that at previous time points, and the area of the low-ozone was also
255 larger.

(a) O$_3$ 0330-UTC00   (b) O$_3$ 0330-UTC02   (c) O$_3$ 0330-UTC04   (d) O$_3$ 0330-UTC06

(e) BrO 0330-UTC00   (f) BrO 0330-UTC02   (g) BrO 0330-UTC04   (h) BrO 0330-UTC06

(i) The geographical map
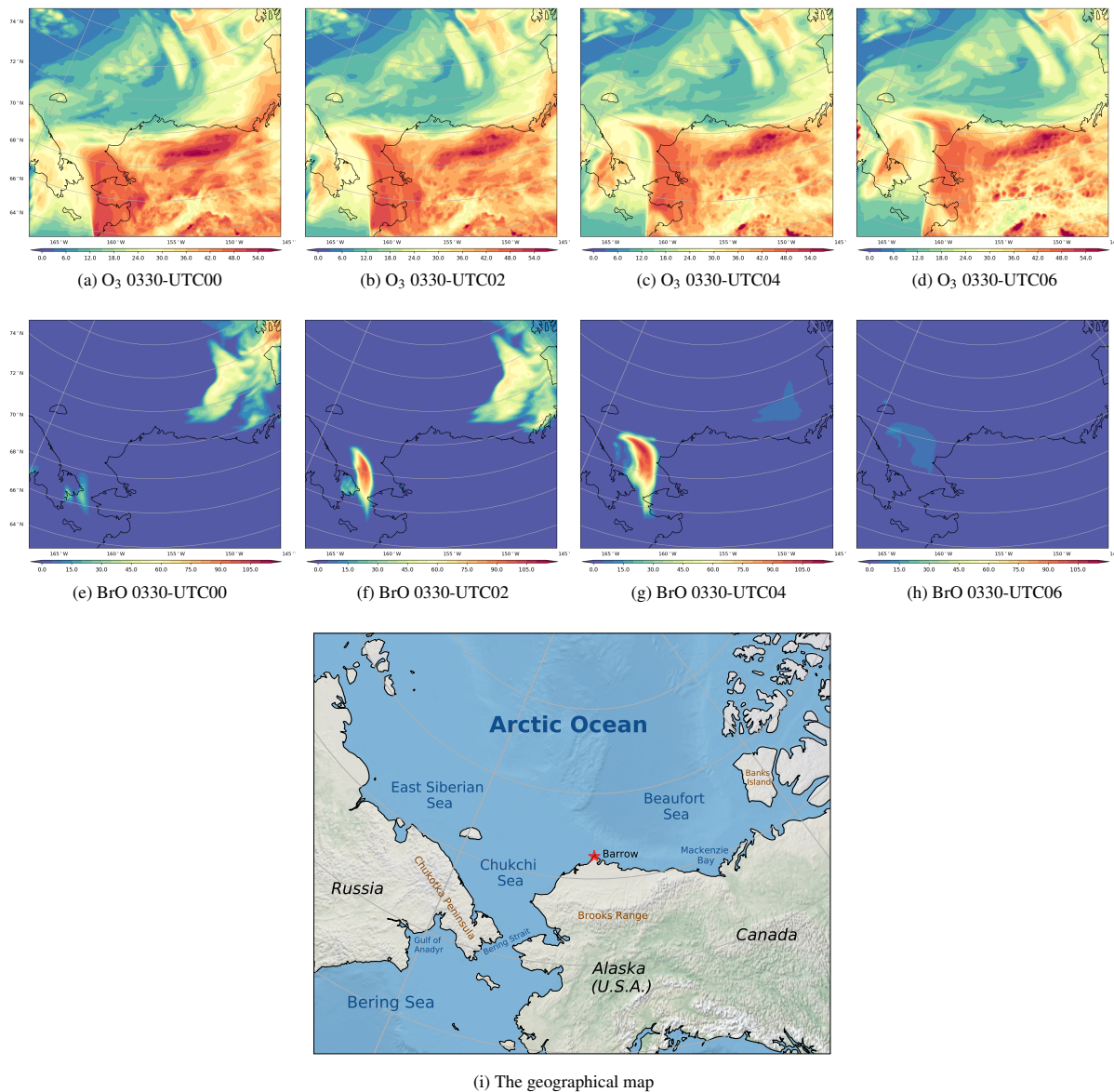
Figure 7. The spatial distribution of the surface ozone (ppb) and BrO (ppt) simulated by CMAQ on March 30th, 2019.

In general, during the time period between March 29th and March 31st, local chemical processes led to the complete ODE over the Beaufort Sea. The center of this ODE was mainly over the north of the Mackenzie Bay, with a maximum of BrO larger than 100 ppt and a minimum of the surface ozone smaller than 5 ppb. As a result, in Barrow, the maximum of BrO reached 21.25 ppt and the minimum of ozone was around 20 ppb. Our simulations agree with the observations of Liao et al. (2012) at Barrow in magnitude, in which the BrO concentration detected in Barrow reached a maximum of 10-20 ppt in the daytime

260

(a) O$_3$ 0330-UTC22   (b) O$_3$ 0331-UTC00   (c) O$_3$ 0331-UTC02   (d) O$_3$ 0331-UTC04

(e) BrO 0330-UTC22   (f) BrO 0331-UTC00   (g) BrO 0331-UTC02   (h) BrO 0331-UTC04

(i) The geographical map
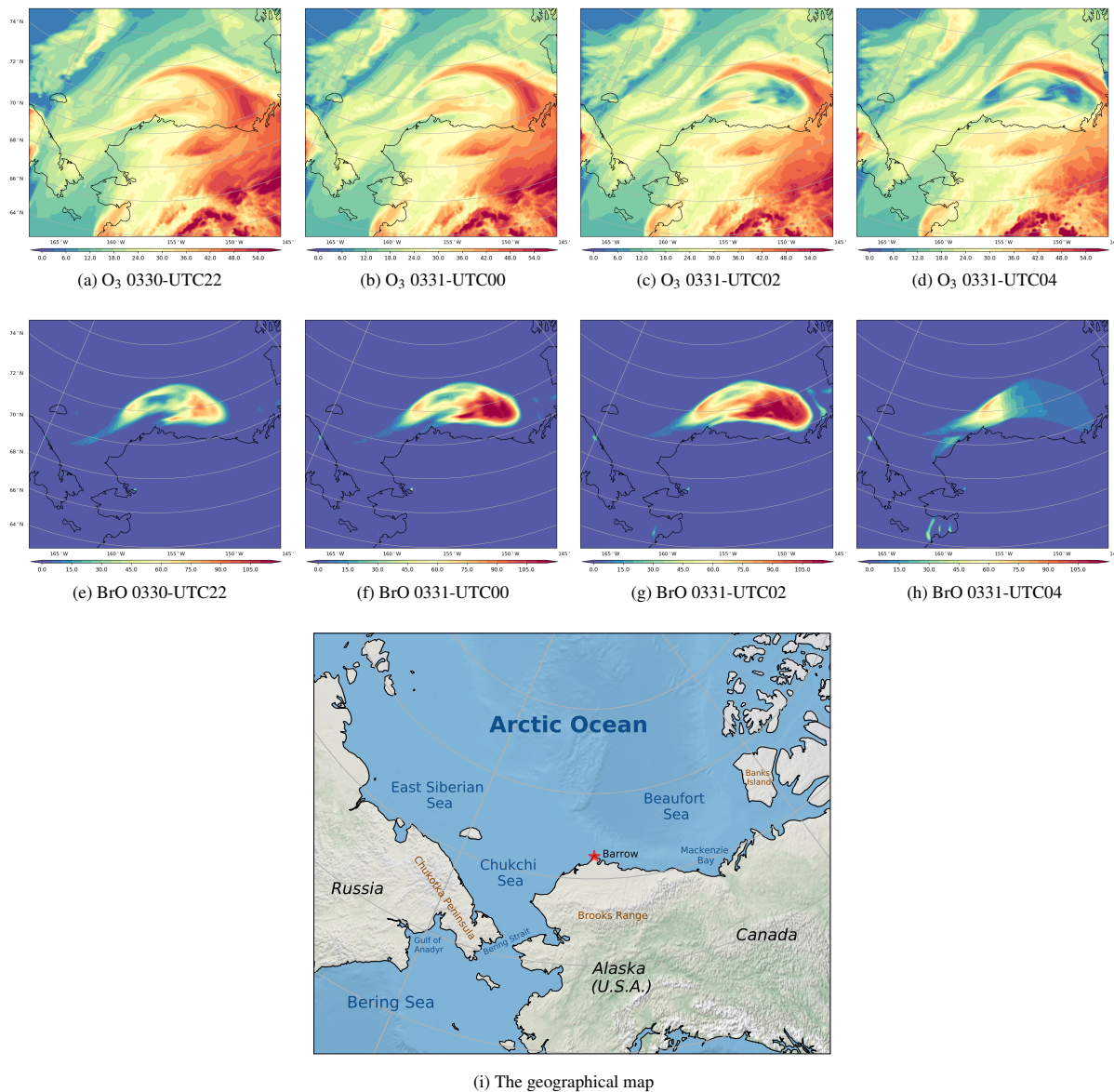
Figure 8. The spatial distribution of the surface ozone (ppb) and BrO (ppt) simulated by CMAQ from March 30th to 31st.

during the ODEs. Thus, we suggested that BrO in the center of the ODE was much larger than that observed at Barrow. Hence, more observations of ozone and bromine over the ocean in the Arctic are required to better understand the properties of ODEs and the bromine explosion mechanism.

The temporal profiles of bromine species and ozone in Barrow are shown in Fig. 9. We can see that the bromine species especially Br$_2$ began to increase on March 30th. After the sunrise, Br$_2$ photolyzed immediately, releasing two bromine atoms.

265
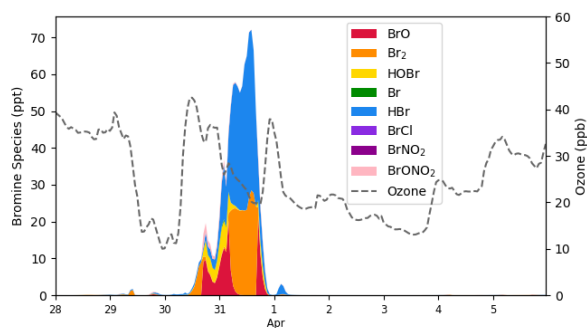
Figure 9. The temporal behavior of bromine species (ppt) and ozone (ppb) simulated by CMAQ in Barrow from March 28th to April 6th, 2019.

These bromine atoms then consumed the surface ozone, forming BrO. Moreover, bromine is continuously released into the atmosphere due to the bromine explosion mechanism. As a result, under this circumstances, ozone began to decrease while BrO burst into the atmosphere. On March 31st, the maximum of BrO in Barrow reached 21.25 ppt in the daytime. Meanwhile, as BrO also reacts with HO_2, forming HOBr, the amount of HOBr also increased during this time. When the sunset occurred,

270   due to the absent of the Br_2 photolysis, BrO declined while HBr and Br_2 accumulated rapidly. The concentration of HBr and Br_2 peaked at 44.7 ppt and 28.5 ppt, respectively. Ozone remained at a relatively low level at this time. Then, sun rose again. Br_2 photolyzed rapidly and BrO was formed again. Afterwards, the air mass in Barrow was carried eastward, the bromine species in Barrow thus declined and the ozone recovered.

3.2.2   ODE2 (on April 2nd)

275   Regarding the ODE occurring on April 2nd (ODE2), we first focused on the weather conditions. During this time, Barrow and its surrounding areas were occupied by a high-pressure system with a cold center from April 2nd to April 4th (see Fig. S6 in the supplements denoting the surface temperature and pressure). Under the control of this high-pressure system, a stable stratification with light anticyclonic winds (less than 5 m/s) was formed in this area. A clear sky, which is a typical weather condition during ODEs (Rancher and Kritz, 1980; Simpson et al., 2007; Anderson and Neff, 2008; Bottenheim et al., 2009; Boylan et al.,

280   2014; Swanson et al., 2020), was also observed. After that, the center of the anticyclone moved slowly southeastward (see Fig. S7 in the supplements for the surface wind fields).

    Under these circumstances, ODEs occurred over the Beaufort Sea and Barrow (see Fig. 10). On April 2nd, due to the existence of the high-pressure system over the Arctic Ocean (see Fig. 10a), Barrow and its surrounding area were controlled by a northerly wind, so that air masses with low ozone from the Arctic Ocean were transported to Barrow. The situation of a

285   low-level surface ozone in Barrow lasted for about one day (Fig. 10b and c). Bottenheim and Chan (2006) also found that under the condition of a strong, stable stratification in the Arctic, it may take more time for the surface ozone recovering from the depleted status, so that the air parcel with depleted ozone can travel a long distance such as from the Arctic Ocean to Barrow. Then, the surface ozone of Barrow recovered to the background level, shown in Fig. 10(d). This ozone recovery was caused by
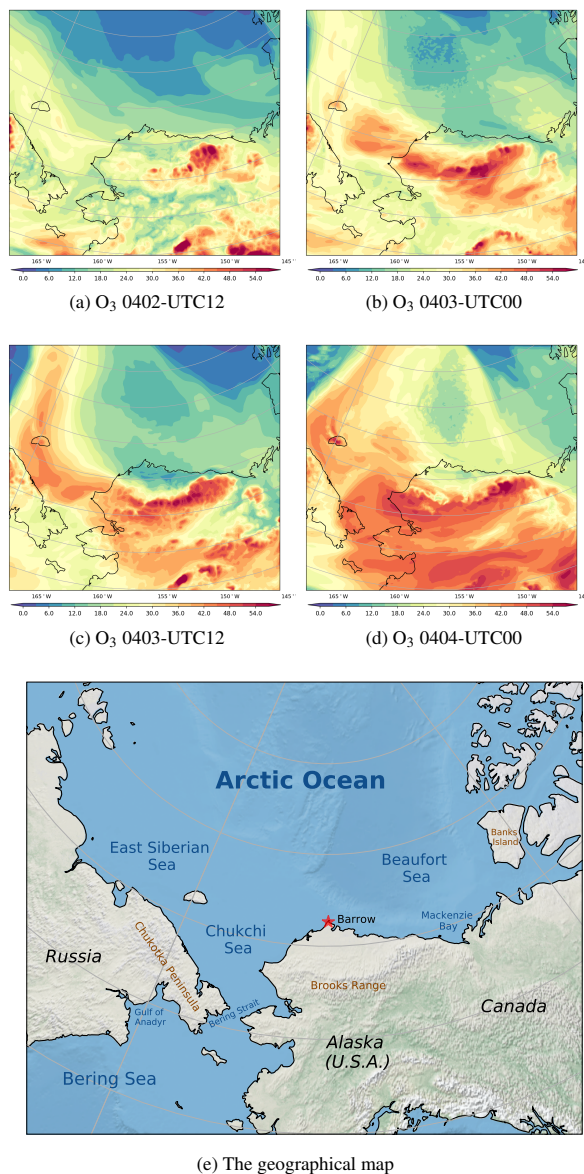
Figure 10. The spatial distribution of the surface ozone (ppb) simulated by CMAQ from April 2nd to 4th, 2019.

a vertical transport of ozone-rich air from the free atmosphere into the boundary layer, which will be shown in a later context.
290 For the variation of the surface ozone with a finer time interval, please refer to Fig. S8 in the supplement.

(a) O_3 (ppb)
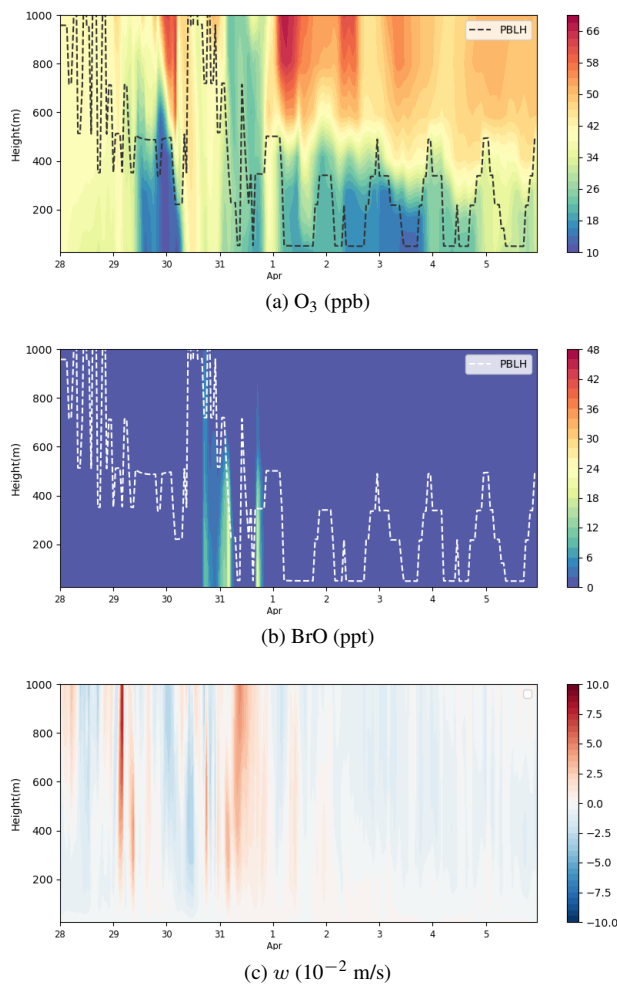
(b) BrO (ppt)

(c) w (10^{-2} m/s)

Figure 11. Vertical profiles of ozone (ppb), BrO (ppt) and vertical wind speed w (10^{-2} m/s) from March 28th to April 6th, 2019 in Barrow, in which the dotted line represents the local planetary boundary layer height (PBLH). A positive w represents an ascending tendency of air parcels while a negative w denotes a descending tendency of air parcels.

3.3 Vertical characteristics

The vertical profiles of ozone, BrO and the vertical wind speed, w, at Barrow below the height of 1000 m are shown in Fig. 11. As described above, during ODE1, a cyclone is formed over the Chukchi Sea and moved northeastward. Thus, at this time stage (on March 30th), the atmospheric activity is intense, and the boundary layer height in Barrow reached 1000 m (see Fig. 11a and b), significantly higher than the typical boundary layer height in Arctic, 100-500 m (Stull, 1988). Meanwhile, the vertical wind speed, w, changed dramatically. The vertical wind speed w was negative on the former half-day of March 30th (see Fig. 11c). Then on the latter half-day, w turned into positive. It denotes a vigorous turbulence in the boundary layer, so that BrO can be

rapidly mixed aloft (see Fig. 11b). On March 31st, w was mostly positive within the whole 1000 m height. BrO was thus carried outside the boundary layer. It led to the occurrence of the partial ODE1 ubiquitously below the height of 1000 m. Therefore, at this time, the depletion of ozone is not limited within the boundary layer, and the ozone in the free atmosphere can also be influenced.

With respect to ODE2 during April 2nd-3rd, from the discussions above, Barrow and its surrounding areas were occupied by a high-pressure system. The boundary layer height in Barrow during this time was lower than that in March, and shows a distinct diurnal variation (see Fig. 11a). Moreover, ozone shows a strong concentration gradient, especially around the top of the boundary layer (see Fig. 11a). The strong concentration gradient was induced by the weak vertical diffusion under the stable stratification. In the study of Bottenheim and Chan (2006), they suggested that the stable stratification would inhibit the recovery of the ozone-lacking status, which corresponded to the case of ODE2. At the end of ODE2, as shown in Fig. 11(c), the vertical wind speed was small but negative within these days. As time went by, ozone in the free troposphere eventually mixed into the boundary layer, and the gradient of ozone is weakened, which represented the end of ODE2.

3.4 Process analysis

We then applied the process analysis (PA), to estimate the contribution from each physical or chemical process to the changes of ozone and bromine species. We first show the ozone change during ODE1 caused by the overall chemistry (see Fig. 12). It can be seen that during the daytime, in most areas, ozone was formed by the chemistry in the presence of sunlight. However, in places where bromine species were activated due to the bromine explosion mechanism, ozone was consumed by the local chemistry. At 02 UTC of March 30th, the chemical consumption of surface ozone reached 6 ppb (see Fig. 12a). At 04 UTC when the sun was setting, the chemical influence disappeared along with the skyline of the sunset (see Fig. 12b). When sun rose again (Fig. 12c), bromine species began to form again under the sunny condition, and the chemical consumption of the surface ozone reached 10 ppb over the Beaufort Sea. However, this strong consumption lasted only a few hours, which declined to 8 ppb at 02 UTC shown in Fig. 12(d). For the chemical contribution to the surface ozone with a finer time interval, please refer to Fig. S9 in the supplement.

In contrast to ODE1, the occurrence of ODE2 is not mainly determined by the local chemistry, so that the chemical contribution to the occurrence of ODE2 is negligible. Thus, we are not showing it in this paper.

We then calculated the contributions from all the physical and chemical processes to the change of ozone and bromine species at Barrow from March 28th to April 6th, 2019, shown in Fig. 13. The vertical transport (including vertical diffusion, vertical advection and dry deposition), horizontal transport (including horizontal diffusion and horizontal advection) were contained.

From Fig. 13(a), it can be seen that the occurrence of ODE1 in Barrow on March 31st was mainly caused by the horizontal transport, which contributed to approximately 6 ppb of the ozone loss. Besides, the recovery of the ODE on March 31st was also owed to the horizontal transport. Thus, during this period, ozone depleted air from ocean was horizontally advected to Barrow, leading to the ozone decline during ODE1. And the termination of ODE1 was caused due to the replenish of ozone-rich air horizontally advected from other areas. Then, during ODE2 on April 2nd, the ozone loss was also found to be largely contributed by the horizontal transport. During the end of ODE2 on April 3rd, a strong vertical transport contributed

(e) The geographical map
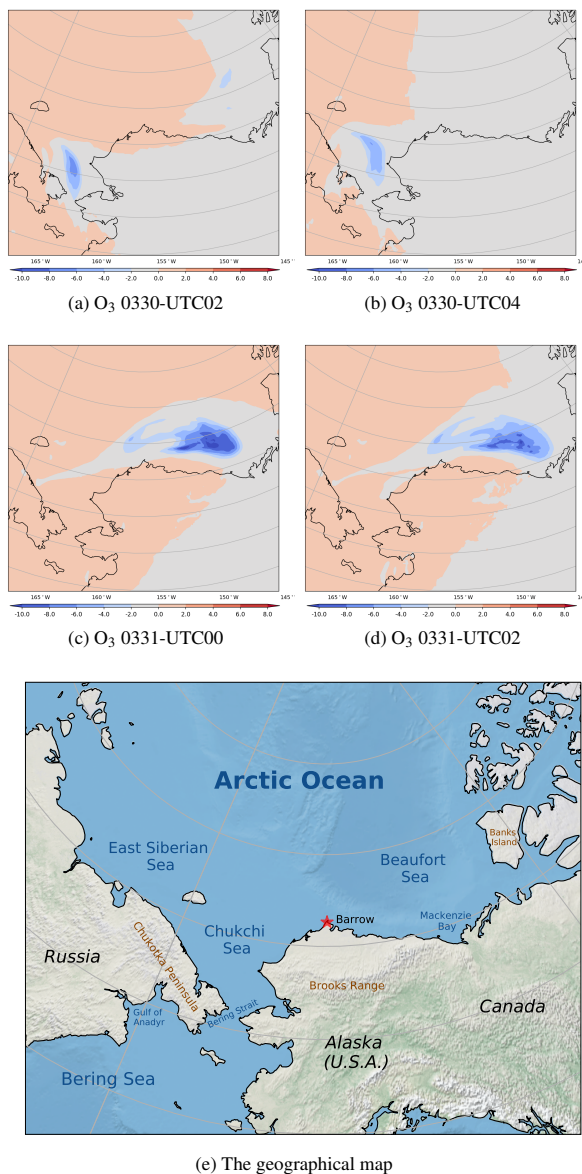
Figure 12. The change of surface ozone (ppb) caused by local chemistry from March 30th to March 31st, 2019. The positive value represents a chemical production of ozone, while the negative value represents a chemical consumption of ozone.

approximately 5 ppb to the ozone recovery, so that the surface ozone can recover to the background level. Thus, the recovery of ODE2 was mainly owed to the vertical transport.

Fig. 13(b) shows the contributions of physical and chemical processes to the change of bromine species during the simulated 335 period. It was found that the variation of the bromine species on March 30th was mainly affected by the chemical process
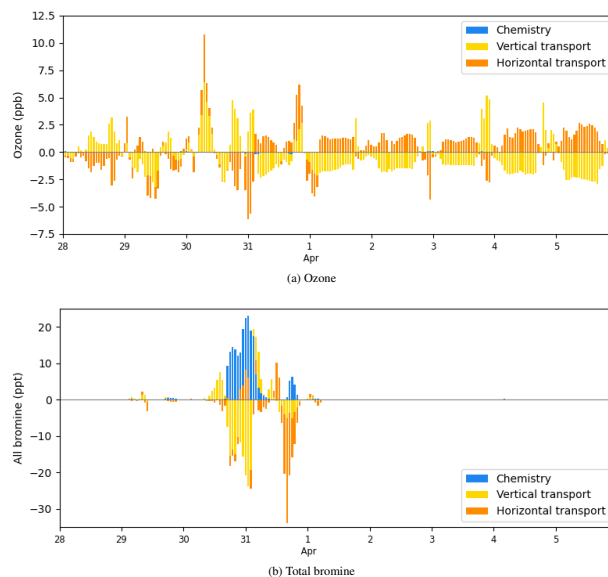
Figure 13. The process analysis of surface ozone and bromine species (Br, Br$_2$, BrO, BrCl, HBr, HOBr, BrNO$_2$ and BrONO$_2$) in Barrow from March 28th to April 6th, 2019.

and vertical transport. The chemical process caused an increase of bromine species by almost 20 ppt. In contrast, the vertical transport contributed at most 25 ppt to the bromine loss, among which the dry deposition was predominant. This was because during ODE1, the cyclone dominates, leading to a strong wind and a vigorous convection within the boundary layer. As a result, the dry deposition velocities of bromine species remarkably increased. Then, on March 31st, the bromine left Barrow
340   mainly due to the horizontal transport.

4   Conclusions and future studies

In this study, we conducted a three-dimensional simulation of ozone depletion events (ODEs) over Barrow and its surrounding areas by using a mesoscale air-quality models, CMAQ, from March 28th to April 6th, 2019. Several ODEs observed at Barrow were captured by the model, and two of them (ODE1 and ODE2) were analyzed thoroughly using process analysis.
345   During ODE1 occurring between March 30th and 31st, a cyclone from the Chukchi Sea traveled to the Beaufort Sea, which provoked a strong wind condition along its trajectory. As a result, a large amount of sea-salt aerosols were released from the Bering Strait, liberating active bromine due to the bromine explosion mechanism. Then the bromine-containing air was carried to the Beaufort Sea, and induced a rapid depletion of surface ozone over the Beaufort Sea. Under the influence of horizontal transport, a partial ODE was observed in Barrow. The termination of this ODE was also due to the horizontal advection of
350   ozone-rich air to Barrow. Regarding ODE2 occurring in Barrow on April 2nd, it was found to be resulted from the transport of

a low-ozone center from the Arctic Sea to Barrow under the influence of a high pressure system. This ozone-lacking status in Barrow then recovered to normal due to a vertical transport of ozone-rich air from the free atmosphere.

From the vertical profiles of ozone, bromine species and wind during these two ODEs, we found that in the presence of a strong uplifting, the ozone-lacking air can be carried to an altitude above the top of the boundary layer, which then influenced the air in the free atmosphere. In contrast, when a stable stratification and a temperature inversion occurred, the low-ozone status would last longer and the air containing depleted ozone can travel further. However, as time passes by, under the influence of a high-pressure system, the impact of the descending air accumulated, so that ozone in the free troposphere eventually mixed into the boundary layer, ending this ODE.

A process analysis (PA) was also used to quantitatively evaluate the contributions of physical and chemical processes to these two ODEs. It showed that the ODE1 in Barrow was mainly caused by the horizontal transport, which contributed to about 6 ppb of the ozone loss. The recovery of this ODE was also largely attributed to the horizontal transport. However, over the sea, the ozone depletion was highly contributed by the chemical process, reaching 6-10 ppb.The process analysis also showed that the ODE occurring on April 2nd (i.e., ODE2) was formed mainly due to the horizontal transport. In contrast, at the end stage of ODE2, a strong vertical transport contributed approximately 5 ppb to the ozone recovery, so that the ozone recovered to the background level. Thus, the recovery of ODE2 was mainly owed to the vertical transport.

Although we well reproduced the ODEs occurring during the spring of 2019 and analyzed the contributions of physicochemical processes to the ODEs, there still exist some limitations for the present study. For instance, the heterogeneous reaction rate representing the bromine explosion mechanism needs a better parameterization. Besides, more observational data would help to further validate our simulations. In addition, simulations for other stations in Arctic are prospected to verify the conclusions achieved in this study.

Code and data availability. The code of the WRF software was obtained from https://www2.mmm.ucar.edu/wrf/users/download/get_sources.html. The code of the CMAQ software was taken from https://github.com/USEPA/CMAQ/. The FNL data were adopted from https://doi.org/10.5065/D65Q4T4Z. Outputs of CAM-Chem model for the implemented boundary conditions of CMAQ were obtained from www.acom.ucar.edu/cam-chem/cam-chem.shtml. The observational data of in-situ meteorology and ozone were provided by the Global Monitoring Laboratory (GML) (https://gml.noaa.gov/aftp/data/barrow/), belonging to the National Oceanic and Atmospheric Administration (NOAA). The surface analysis was obtained from Weather Prediction Center (www.wpc.ncep.noaa.gov/html/sfc-zoom.php). The code for changing the boundary conditions of CMAQ can be found in https://github.com/Simeng-unique/acp-supplements.

Video supplement. The video supplement related to this article can be found in https://github.com/Simeng-unique/acp-supplements.

Author contributions. Le Cao conceived the idea of the article. Simeng Li configured and performed the computations. Simeng also revised
380 the chemical mechanisms and wrote the paper together with Le Cao. Yicheng Gu and Yuhan Luo participated in discussions and gave
valuable suggestions on the improvement of the manuscript. All the authors listed read and approved the final manuscript.

Competing interests. The authors declare that they have no conflict of interest.

Acknowledgements. Numerical calculations in this paper have been performed on the high-performance computing system in the High
Performance Computing Center, Nanjing University of Information Science & Technology. The authors also like to thank Barron Henderson
385 and Golam Sarwar from U.S. EPA sincerely for helping us dealing with ocean file, which is to be used in a future study using CMAQ v5.3.2.

Financial support. This research has been supported by the National Natural Science Foundation of China (grant no. 41705103).

References

Anderson, P. S. and Neff, W. D.: Boundary layer physics over snow and ice, Atmospheric Chemistry and Physics, 8, 3563–3582, https://doi.org/10.5194/acp-8-3563-2008, 2008.

390 Baek, B. and Seppanen, C.: CEMPD/SMOKE: SMOKE v4.7 Public Release (October 2019), https://doi.org/10.5281/zenodo.3476744, 2019.

Barrie, L. A., Bottenheim, J. W., Schnell, R. C., Crutzen, P. J., and Rasmussen, R. A.: Ozone destruction and photochemical reactions at polar sunrise in the lower Arctic atmosphere, Nature, 334, 138–141, https://doi.org/10.1038/334138a0, 1988.

Blechschmidt, A.-M., Richter, A., Burrows, J. P., Kaleschke, L., Strong, K., Theys, N., Weber, M., Zhao, X., and Zien, A.: An exemplary case of a bromine explosion event linked to cyclone development in the Arctic, Atmospheric Chemistry and Physics, 16, 1773–1788,
395 https://doi.org/10.5194/acp-16-1773-2016, 2016.

Bottenheim, J. W. and Chan, E.: A trajectory study into the origin of spring time Arctic boundary layer ozone depletion, Journal of Geophysical Research: Atmospheres, 111, https://doi.org/10.1029/2006JD007055, 2006.

Bottenheim, J. W., Barrie, L. A., Atlas, E., Heidt, L. E., Niki, H., Rasmussen, R. A., and Shepson, P. B.: Depletion of lower tropospheric ozone during Arctic spring: The Polar Sunrise Experiment 1988, Journal of Geophysical Research: Atmospheres, 95, 18 555–18 568,
400 https://doi.org/10.1029/JD095iD11p18555, 1990.

Bottenheim, J. W., Netcheva, S., Morin, S., and Nghiem, S. V.: Ozone in the boundary layer air over the Arctic Ocean: measurements during the TARA transpolar drift 2006–2008, Atmospheric Chemistry and Physics, 9, 4545–4557, https://doi.org/10.5194/acp-9-4545-2009, 2009.

Boylan, P., Helmig, D., Staebler, R., Turnipseed, A., Fairall, C., and Neff, W.: Boundary layer dynamics during the Ocean-
405 Atmosphere-Sea-Ice-Snow (OASIS) 2009 experiment at Barrow, AK, Journal of Geophysical Research: Atmospheres, 119, 2261–2278, https://doi.org/10.1002/2013JD020299, 2014.

Buchholz, R. R., Emmon, L. K., Tilmes, S., and The CESM2 Development Team: CESM2.1/CAM-chem Instantaneous Output for Boundary Conditions, Tech. rep., UCAR/NCAR - Atmospheric Chemistry Observations and Modeling Laboratory, 10.5065/NMP7-EP60, subset used Lat: 20 to 88, Lon: -180 to -130, March 2019 - April 2019, Accessed 27 Apr 2021, 2019.

410 Chen, F., Janjić, Z., and Mitchell, K.: Impact of Atmospheric Surface-layer Parameterizations in the new Land-surface Scheme of the NCEP Mesoscale Eta Model, Boundary-Layer Meteorology, 85, 391–421, https://doi.org/10.1023/A:1000531001463, 1997.

Crippa, M., Guizzardi, D., Muntean, M., Schaaf, E., Dentener, F., van Aardenne, J. A., Monni, S., Doering, U., Olivier, J. G. J., Pagliari, V., and Janssens-Maenhout, G.: Gridded emissions of air pollutants for the period 1970–2012 within EDGAR v4.3.2, Earth System Science Data, 10, 1987–2013, https://doi.org/10.5194/essd-10-1987-2018, 2018.

415 Crippa, M., Solazzo, E., Huang, G., and et al.: High resolution temporal profiles in the Emissions Database for Global Atmospheric Research, Sci Data, 7, https://doi.org/10.1038/s41597-020-0462-2, 2020.

Emmons, L. K., Schwantes, R. H., Orlando, J. J., Tyndall, G., Kinnison, D., Lamarque, J.-F., Marsh, D., Mills, M. J., Tilmes, S., Bardeen, C., Buchholz, R. R., Conley, A., Gettelman, A., Garcia, R., Simpson, I., Blake, D. R., Meinardi, S., and Pétron, G.: The Chemistry Mechanism in the Community Earth System Model Version 2 (CESM2), Journal of Advances in Modeling Earth Systems, 12, e2019MS001 882,
420 https://doi.org/10.1029/2019MS001882, 2020.

Fan, S.-M. and Jacob, D.: Surface ozone depletion in Arctic spring sustained by bromine reactions on aerosols, Nature, 359, 522–524, https://doi.org/10.1038/359522a0, 1992.

Gipson, G. L.: Chapter 16: Process analysis, Science Algorithms of the EPA Models-3 Community Multiscale Air Quality (CMAQ) Modeling
System, https://nepis.epa.gov/Exe/ZyPURL.cgi?Dockey=30003R9Y.txt, ePA/600/R-99/030, 1999.

425 Hausmann, M. and Platt, U.: Spectroscopic measurement of bromine oxide and ozone in the high Arctic during Polar Sunrise Experiment
1992, Journal of Geophysical Research: Atmospheres, 99, 25 399–25 413, https://doi.org/10.1029/94JD01314, 1994.

Herbert, G., Green, E., Harris, J., Koenig, G., Roughton, S., and Thaut, K.: Control and Monitoring Instrumentation for the Continuous
Measurement of Atmospheric CO_2 and Meteorological Variables, Journal of Atmospheric and Oceanic Technology, 3, 414–421, 1986a.

Herbert, G., Green, E., Koenig, G., and Thaut, K.: Monitoring instrumentation for the continuous measurement and quality assurance of
430 meteorological observations, Tech. rep., NOAA Tech. Memo. ERL ARL-148, 1986b.

Herbert, G., Harris, J., Bieniulis, M., and McCutcheon, J.: Acquisition and Data Management, in CMDL Summary Report 1989, Tech.
Rep. 18, 1990.

Herbert, G., Bieniulis, M., Mefford, T., and Thaut, K.: Acquisition and Data Management Division, in CMDL Summary Report 1993, Tech.
Rep. 22, 1994.

435 Herrmann, M., Sihler, H., Frieß, U., Wagner, T., Platt, U., and Gutheil, E.: Time-dependent 3D simulations of tropospheric ozone depletion
events in the Arctic spring using the Weather Research and Forecasting model coupled with Chemistry (WRF-Chem), Atmospheric
Chemistry and Physics, 21, 7611–7638, https://doi.org/10.5194/acp-21-7611-2021, 2021.

Herrmann, M., Schöne, M., Borger, C., Warnach, S., Wagner, T., Platt, U., and Gutheil, E.: Ozone depletion events in the Arctic
spring of 2019: A new modeling approach to bromine emissions, Atmospheric Chemistry and Physics Discussions, 2022, 1–39,
440 https://doi.org/10.5194/acp-2022-334, 2022.

Iacono, M. J., Delamere, J. S., Mlawer, E. J., Shephard, M. W., Clough, S. A., and Collins, W. D.: Radiative forcing by long-
lived greenhouse gases: Calculations with the AER radiative transfer models, Journal of Geophysical Research: Atmospheres, 113,
https://doi.org/10.1029/2008JD009944, 2008.

Janjić, Z. I.: The Step-Mountain Eta Coordinate Model: Further Developments of the Convection, Viscous Sublayer Turbulence Closure
445 Schemes, Monthly Weather Review, 122, 927 – 945, https://doi.org/10.1175/1520-0493(1994)122<0927:TSMECM>2.0.CO;2, 1994.

Lehrer, E., Hönninger, G., and Platt, U.: A one dimensional model study of the mechanism of halogen liberation and vertical transport in the
polar troposphere, Atmospheric Chemistry and Physics, 4, 2427–2440, https://doi.org/10.5194/acp-4-2427-2004, 2004.

Liao, J., Huey, L. G., Tanner, D. J., Flocke, F. M., Orlando, J. J., Neuman, J. A., Nowak, J. B., Weinheimer, A. J., Hall, S. R., Smith, J. N.,
Fried, A., Staebler, R. M., Wang, Y., Koo, J.-H., Cantrell, C. A., Weibring, P., Walega, J., Knapp, D. J., Shepson, P. B., and Stephens, C. R.:
450 Observations of inorganic bromine (HOBr, BrO andBr2) speciation at Barrow, Alaska, in spring 2009, Journal of Geophysical Research:
Atmospheres, 117, https://doi.org/10.1029/2011JD016641, 2012.

Marelle, L., Thomas, J. L., Ahmed, S., Tuite, K., Stutz, J., Dommergue, A., Simpson, W. R., Frey, M. M., and Baladima, F.: Implementation
and Impacts of Surface and Blowing Snow Sources of Arctic Bromine Activation Within WRF-Chem 4.1.1, Journal of Advances in
Modeling Earth Systems, 13, e2020MS002 391, https://doi.org/10.1029/2020MS002391, 2021.

455 McClure-Begley, A., Petropavlovskikh, I., and Oltmans, S.: NOAA Global Monitoring Surface Ozone Network,
https://doi.org/10.7289/V57P8WBF, 2014.

McConnell, J. C., Henderson, G. S., Barrie, L., Bottenheim, J., Niki, H., Langford, C. H., and Templeton, E. M. J.: Photochemical bromine
production implicated in Arctic boundary-layer ozone depletion, Nature, 355, 150–152, https://doi.org/10.1038/355150a0, 1992.

Mefford, T., Bieniulis, M., Halter, B., and Peterson, J.: Meteorological Measurements, in CMDL Summary Report 1994 - 1995, Tech.
460 Rep. 23, 1996.

Mellberg, J.: Final Report Ozone Depletion by Bromine and Iodine over the Gulf of Mexico, Tech. rep., Texas Commission on Environmental Quality, 2014.

Monforti-Ferrario, F., Oreggioni, G., Schaaf, E., Guizzardi, D., Olivier, J., Solazzo, E., Lo Vullo, E., Crippa, M., Muntean, M., and Vignati, E.: Fossil CO2 and GHG emissions of all world countries, https://doi.org/10.2760/687800, 2019.

465 National Centers for Environmental Prediction, National Weather Service, NOAA, and U.S. Department of Commerce: NCEP GDAS/FNL 0.25 Degree Global Tropospheric Analyses and Forecast Grids, 10.5065/D65Q4T4Z, 2015.

Oltmans, S. J.: Surface ozone measurements in clean air, Journal of Geophysical Research: Oceans, 86, 1174–1180, https://doi.org/10.1029/JC086iC02p01174, 1981.

Pesaresi, M., Florczyk, A., Schiavina, M., Melchiorri, M., and Maffenini, L.: GHS-SMOD R2019A - GHS settlement layers, updated and
470 refined REGIO model 2014 in application to GHS-BUILT R2018A and GHS-POP R2019A, multitemporal (1975-1990-2000-2015), Tech. rep., European Commission, Joint Research Centre (JRC), https://doi.org/10.2905/42E8BE89-54FF-464E-BE7B-BF9E64DA5218, 2019.

Platt, U. and Hönninger, G.: The role of halogen species in the troposphere, Chemosphere, 52, 325–338, https://doi.org/10.1016/S0045-6535(03)00216-9, naturally Produced Organohalogens, 2003.

Platt, U. and Lehrer, E.: Arctic tropospheric ozone chemistry - ARCTOC : results from field, laboratory and modelling studies : final report
475 of the EU project Contract No EV5V-V-CT93-0318(DTEF), Luxembourg, 1997.

Rancher, J. and Kritz, M. A.: Diurnal fluctuations of Br and I in the tropical marine atmosphere, Journal of Geophysical Research: Oceans, 85, 5581–5587, https://doi.org/10.1029/JC085iC10p05581, 1980.

Sarwar, G., Gantt, B., Schwede, D., Foley, K., Mathur, R., and Saiz-Lopez, A.: Impact of Enhanced Ozone Deposition and Halogen Chemistry on Tropospheric Ozone over the Northern Hemisphere, Environmental Science & Technology, 49, 9203–9211,
480 https://doi.org/10.1021/acs.est.5b01657, 2015.

Seinfeld, J. H. and Pandis, S. N.: Atmospheric Chemistry and Physics: From Air Pollution to Climate Change, John Wiley & Sons, third edition edn., 2016.

Sherwen, T., Evans, M. J., Carpenter, L. J., Andrews, S. J., Lidster, R. T., Dix, B., Koenig, T. K., Sinreich, R., Ortega, I., Volkamer, R., Saiz-Lopez, A., Prados-Roman, C., Mahajan, A. S., and nez, C. O.: Iodine's impact on tropospheric oxidants: a global model study
485 in GEOS-Chem, Atmospheric Chemistry and Physics, 16, 1161–1186, https://doi.org/10.5194/acp-16-1161-2016, 2016.

Simpson, W. R., von Glasow, R., Riedel, K., Anderson, P., Ariya, P., Bottenheim, J., Burrows, J., Carpenter, L. J., Frieß, U., Goodsite, M. E., Heard, D., Hutterli, M., Jacobi, H.-W., Kaleschke, L., Neff, B., Plane, J., Platt, U., Richter, A., Roscoe, H., Sander, R., Shepson, P., Sodeau, J., Steffen, A., Wagner, T., and Wolff, E.: Halogens and their role in polar boundary-layer ozone depletion, Atmospheric Chemistry and Physics, 7, 4375–4418, https://doi.org/10.5194/acp-7-4375-2007, 2007.

490 Skamarock, W. C., Klemp, J. B., and J. Dudhia, e. a.: A Description of the Advanced Research WRF Version 3, Tech. rep., University Corporation for Atmospheric Research, https://doi.org/http://dx.doi.org/10.5065/D68S4MVH, 2008.

Steffen, A., Douglas, T., Amyot, M., Ariya, P., Aspmo, K., Berg, T., Bottenheim, J., Brooks, S., Cobbett, F., Dastoor, A., Dommergue, A., Ebinghaus, R., Ferrari, C., Gardfeldt, K., Goodsite, M. E., Lean, D., Poulain, A. J., Scherz, C., Skov, H., Sommar, J., and Temme, C.: A synthesis of atmospheric mercury depletion event chemistry in the atmosphere and snow, Atmospheric Chemistry and Physics, 8,
495 1445–1482, https://doi.org/10.5194/acp-8-1445-2008, 2008.

Stull, R. B.: An Introduction to Boundary Layer Meteorology, Springer, Dordrecht, https://doi.org/10.1007/978-94-009-3027-8, 1988.

Swanson, W., Graham, K. A., Halfacre, J. W., Holmes, C. D., Shepson, P. B., and Simpson, W. R.: Arctic Reactive Bromine Events Occur in Two Distinct Sets of Environmental Conditions: A Statistical Analysis of 6 Years of Observations, Journal of Geophysical Research: Atmospheres, 125, e2019JD032 139, https://doi.org/10.1029/2019JD032139, 2020.

500 Thomas, J. L., Stutz, J., Lefer, B., Huey, L. G., Toyota, K., Dibb, J. E., and von Glasow, R.: Modeling chemistry in and above snow at Summit, Greenland – Part 1: Model description and results, Atmospheric Chemistry and Physics, 11, 4899–4914, https://doi.org/10.5194/acp-11-4899-2011, 2011.

Thomas, J. L., Dibb, J. E., Huey, L. G., Liao, J., Tanner, D., Lefer, B., von Glasow, R., and Stutz, J.: Modeling chemistry in and above snow at Summit, Greenland – Part 2: Impact of snowpack chemistry on the oxidation capacity of the boundary layer, Atmospheric Chemistry 505 and Physics, 12, 6537–6554, https://doi.org/10.5194/acp-12-6537-2012, 2012.

Thompson, G., Field, P. R., Rasmussen, R. M., and Hall, W. D.: Explicit Forecasts of Winter Precipitation Using an Improved Bulk Microphysics Scheme. Part II: Implementation of a New Snow Parameterization, Monthly Weather Review, 136, 5095 – 5115, https://doi.org/10.1175/2008MWR2387.1, 2008.

Tiedtke, M.: A Comprehensive Mass Flux Scheme for Cumulus Parameterization in Large-Scale Models, Monthly Weather Review, 117, 510 1779 – 1800, https://doi.org/10.1175/1520-0493(1989)117<1779:ACMFSF>2.0.CO;2, 1989.

US EPA Office of Research and Development: CMAQ, https://doi.org/10.5281/zenodo.1212601, For up-to-date documentation, source code, and sample run scripts, please clone or download the CMAQ git repository available through GitHub: https://github.com/USEPA/CMAQ/tree/5.2.1, 2018.

US EPA Office of Research and Development: CMAQ, https://doi.org/10.5281/zenodo.4081737, For up-to-date documentation, source code, 515 and sample run scripts, please clone or download the CMAQ git repository available through GitHub: https://github.com/USEPA/CMAQ, 2020.

von Glasow, R. and Crutzen, P.: 5.2 - Tropospheric Halogen Chemistry, in: Treatise on Geochemistry (Second Edition), edited by Holland, H. D. and Turekian, K. K., pp. 19–69, Elsevier, Oxford, second edition edn., https://doi.org/10.1016/B978-0-08-095975-7.00402-2, 2014.

Wennberg, P. O.: Bromine Explosion, Nature, 397, 299–301, https://doi.org/10.1038/16805, 1999.

520 Yang, X., Pyle, J. A., and Cox, R. A.: Sea salt aerosol production and bromine release: Role of snow on sea ice, Geophysical Research Letters, 35, https://doi.org/10.1029/2008GL034536, 2008.

Yang, X., Pyle, J. A., Cox, R. A., Theys, N., and Van Roozendael, M.: Snow-sourced bromine and its implications for polar tropospheric ozone, Atmospheric Chemistry and Physics, 10, 7763–7773, https://doi.org/10.5194/acp-10-7763-2010, 2010.

Yang, X., Frey, M. M., Rhodes, R. H., Norris, S. J., Brooks, I. M., Anderson, P. S., Nishimura, K., Jones, A. E., and Wolff, E. W.: Sea 525 salt aerosol production via sublimating wind-blown saline snow particles over sea ice: parameterizations and relevant microphysical mechanisms, Atmospheric Chemistry and Physics, 19, 8407–8424, https://doi.org/10.5194/acp-19-8407-2019, 2019.

Yarwood, G., Jung, J., Nopmongcol, O., and Emery, C.: Final Report Improving CAMx Performance in Simulating Ozone Transport from the Gulf of Mexico, Tech. rep., Texas Commission on Environmental Quality, 2012.

Zeng, T., Wang, Y., Chance, K., Browell, E. V., Ridley, B. A., and Atlas, E. L.: Widespread persistent near-surface ozone depletion at northern 530 high latitudes in spring, Geophysical Research Letters, 30, https://doi.org/10.1029/2003GL018587, 2003.

Zeng, T., Wang, Y., Chance, K., Blake, N., Blake, D., and Ridley, B.: Halogen-driven low-altitude O3 and hydrocarbon losses in spring at northern high latitudes, Journal of Geophysical Research: Atmospheres, 111, https://doi.org/10.1029/2005JD006706, 2006.